

Termination dependence of the surface states in Pb_2Pd

Surajit Basak^{1,*} and Andrzej Ptok^{1,†}

¹*Institute of Nuclear Physics, Polish Academy of Sciences, W. E. Radzikowskiego 152, PL-31342 Kraków, Poland*
(Dated: August 19, 2022)

Topological properties of systems lead to the emergence of surface states which can be observed experimentally within the angle-resolved photoemission spectroscopy (ARPES) measurements. Recently, the topological properties of Pb_2Pd were reported. In this paper, we discuss the role of the surface termination on the realized surface states. We discuss the termination dependence of the surface state for (001) and (110) surface. We demonstrate that the Pd terminated (001) surface allow realization of the Dirac cone-like surface state. In the case (110) we observe well visible surface states with parabolic-like dispersion relation in close vicinity of the Fermi level.

I. INTRODUCTION

The surface states and their topological behaviors were intensively investigated in past years [1, 2]. Best example of such states are the “metallic” surface states observed experimentally within the angle-resolved photoemission spectroscopy (ARPES) in the topological insulators [3–5]. The topological surface states preserve their properties also in presence of the magnetic impurities [6–8], and that in the presence of intrinsic magnetism can be source of new classes of magnetic topological insulators [9–12]. More recently, realization of the Dirac [13–15], Weyl [16–20], or nodal line [21–27] semimetals have drawn a lot of attention too.

Metallic systems can also exhibit the topological properties. One such example is Pb_2Pd , which was first recognized as a superconductor in 1962 [28]. Powder XRD measurements confirm realization of the $I4/mcm$ space group [29]. System remained the same after Bi-doping and the cell volume monotonically increased with higher Bi content [30]. Similarly to PdTe_2 [31], Pb_2Pd exhibit conventional *s-wave* superconducting behavior of the specific heat jump at T_c around 3 K [28, 29, 32].

Independent of the realized symmetry, the Pd-compounds (like PdAu_2 [33], PdSb_2 [34], PdTe_2 [35–38], or PdBi_2 [39, 40]) typically exhibit topological properties.

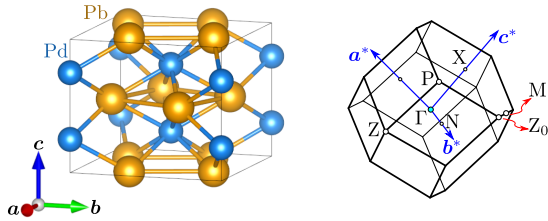


FIG. 1. Crystal structure of Pb_2Pd with $I4/mcm$ symmetry (left), and the corresponding Brillouin zone with their high symmetry points (right).

For example, in case of PdTe_2 (with $P\bar{3}m1$ symmetry) the bulk Dirac point and topological surface states were reported [35–38]. Initial theoretical results also suggest topological properties in the case of Pb_2Pd [29], however, this feature is yet to be studied properly. In this paper, we discuss the electronic properties of Pb_2Pd (electronic bulk band structure, and termination dependence of the surface states). This paper is organized as follows. In Sec. II we present and discuss our numerical results, which are concluded in Sec. III.

II. NUMERICAL RESULTS AND DISCUSSION

A. Calculations details

The first-principle calculations were performed within density-functional theory (DFT) using the projector augmented-wave (PAW) method [41] implemented in the Vienna *Ab initio* Simulation Package (VASP) [42–44]. The exchange-correlation potential was obtained by the generalized gradient approximation (GGA) in the form proposed by Perdew, Burke, and Enzerhof (PBE) [45]. The energy cut-off for the plane-wave expansion was equal to 400 eV. The optimization of the conventional cell was performed using a $12 \times 12 \times 12$ Monkhorst-Pack \mathbf{k} -grid [46]. The structures were relaxed using the conjugate gradient technique with the energy convergence criteria set at 10^{-8} eV and 10^{-6} eV for the electronic and ionic iterations, respectively. Symmetry of the structures were analyzed with FINDSYM [47] and SEEK-PATH [48, 49] packages.

Using results of the DFT calculation for electronic band structure we can find the tight binding model in the basis of the maximally localized Wannier orbitals [50–52]. It can be performed via the WANNIER90 software [53–55]. In our calculations, we used the $10 \times 10 \times 10$ full \mathbf{k} -point DFT calculation, starting from *p* orbitals for Pb atoms, *p* and *d* orbitals for Pd atoms. This gives us 28-orbital tight binding model of the Pb_2Pd . Finally, to study the surface states, the surface Green’s function for semi-infinite system [56] was calculated using WANNIERTOOLS [57].

* e-mail: surajit.basak@ifj.edu.pl

† e-mail: aptok@mmj.pl

B. Crystal structure

Pb_2Pd crystallize with $I4/mcm$ symmetry (space group No. 140), i.e. a body-centered tetragonal unit cell with Pd atoms at the body center. After the DFT optimization, the lattice constants were found to be $a = b = 6.997 \text{ \AA}$, and $c = 5.920 \text{ \AA}$, which are close to the experimentally reported values $a = b = 6.863 \text{ \AA}$, and $c = 5.840 \text{ \AA}$ [29]. The Pd and Pb atoms are located in the high symmetry Wyckoff positions $4a$ (0,0,0.25), and $8h$ (0.1630,0.6630,0), respectively. Here it should be noted that the experimentally obtained Pb atom position was (0.1643,0.6643,0), which is close to the theoretical one [29].

C. Bulk electronic band structure

The bulk electronic band structure is presented in Fig. 2 (orange and blue lines correspond to the results in the absence and presence of the spin-orbit coupling, respectively). In the band structure, several nearly-flat bands (approximately 2 eV below the Fermi level) can be distinguished. However, around the Fermi level, the bands exhibit strong dispersion.

This spin-orbit coupling lead to lift the band degeneracy. This is well visible, e.g., at the Γ point, where splitting is in range of 0.5 eV. However, largest impact of the spin-orbit coupling on the band structure is visible mostly above the Fermi level – e.g. at M point, around 2 eV above the Fermi level, where the strong band structure is observed.

Four bands forming the Fermi surface (Fig. 3) have electronic character. First two bands, with nearly parabolic-like dispersion relation around Γ point, create

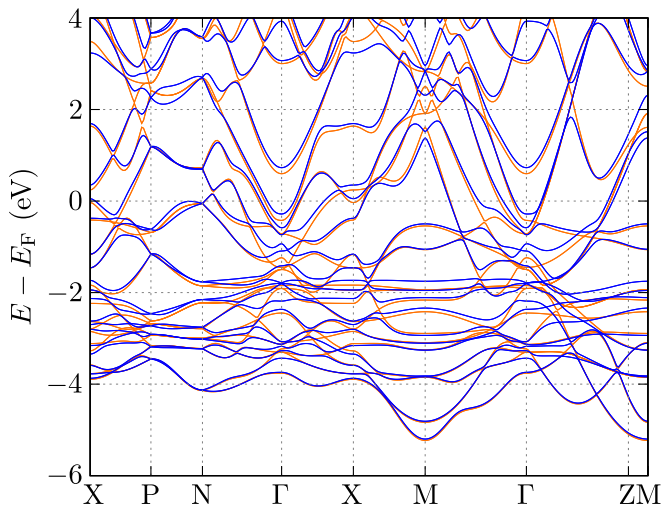


FIG. 2. Bulk electronic band structure of Pb_2Pd with $I4/mcm$ symmetry. The orange and blue line show results in the absence and presence of the spin-orbit coupling, respectively.

two sphere-like pockets [Fig. 3(c) and (d)]. Next two

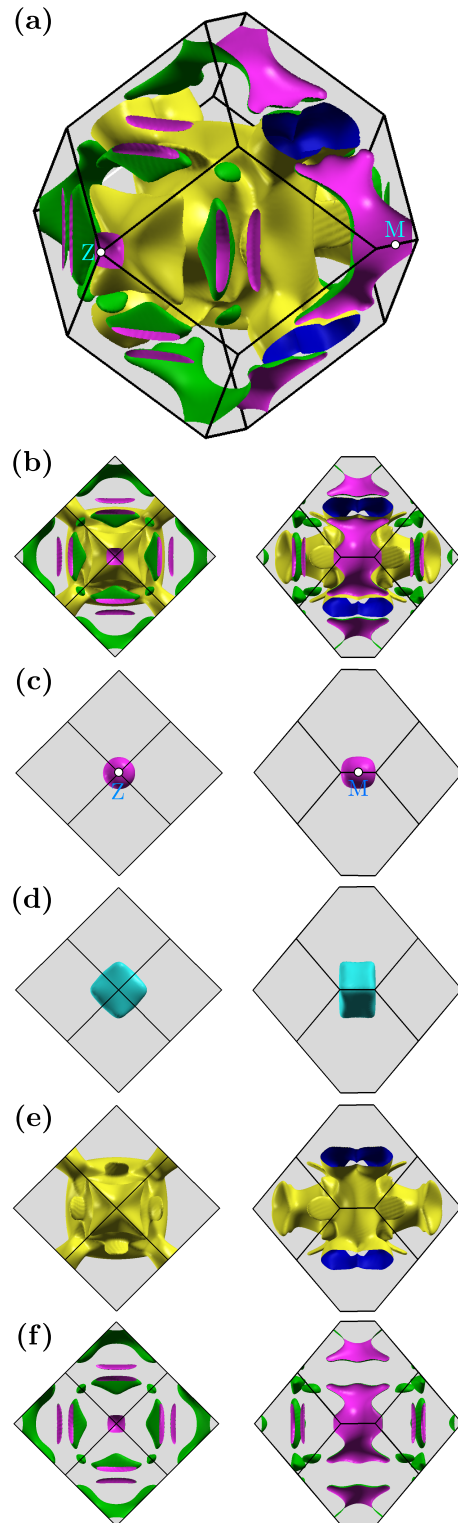


FIG. 3. The Fermi surface of Pb_2Pd with $I4/mcm$ symmetry, in the presence of the spin-orbit coupling. Panels (a) and (b) present the full Fermi surface, while panels (c)–(f) present the separate pockets.

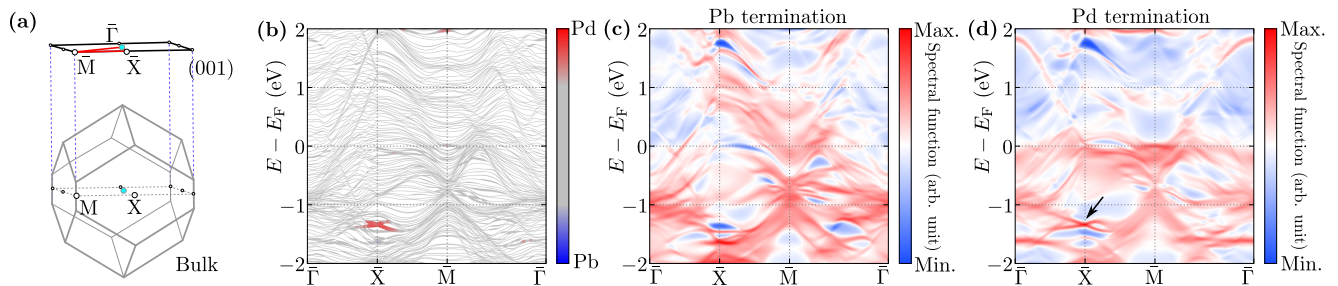


FIG. 4. (a) Projection of the bulk Brillouin zone on the (001) surface of the Brillouin zone. (b) Electronic band structure from the slab-type calculation. Color correspond to the contribution of the surface with different type of terminations (as labeled). In panels (c) and (d), the surface spectral function for different surface terminations are presented (as labeled).

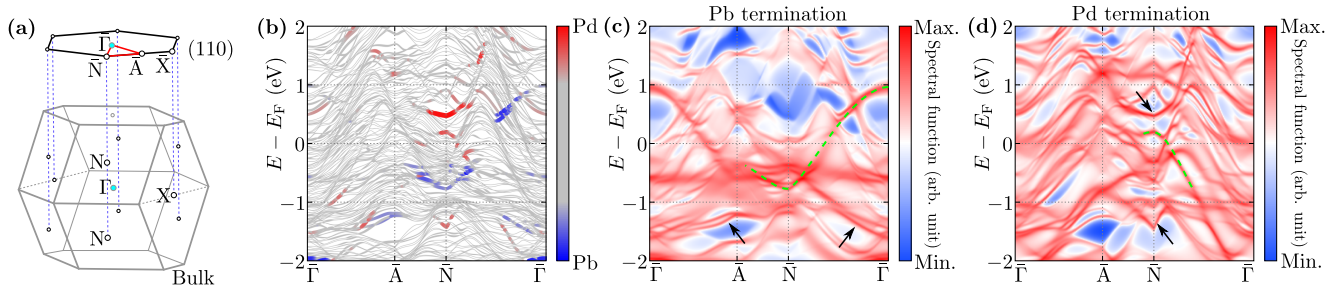


FIG. 5. (a) Projection of the bulk Brillouin zone on the (110) surface of the Brillouin zone. (b) Electronic band structure from the slab-type calculation. Color correspond to the contribution of the surface with different type of termination (as labeled). In panels (c) and (d), the surface spectral function for different surface terminations are presented (as labeled).

bands present strong \mathbf{k} -dependence [Fig. 3(e) and (f)].

D. Surface states

Now, we will present analyses of the surface states for (001) and (110) surfaces (Fig. 4 and Fig. 5, respectively), which hosts the surface states in close vicinity of the Fermi level.

The electronic band structure calculated for the slab geometry [panels (b)] presents a very complex structure [blue to the projection of the 3D bulk Brillouin zone to 2D surface Brillouin zone, presented in panels (a)]. Absence of periodic boundary conditions along the direction parallel to the surface allow realization of the surface states as a consequence dangling bonds of the atoms on the surface. Indeed, direct analyses of the band projection on the surface atoms reflects the presence of the surface states [color contours on panels (b)]. The realized geometry allows us to find the surface states realized by the surface terminated by the Pb atoms (blue color), as well as by the Pd atoms (red color). As we can see, in case of the (001) surface [Fig. 4(b)], the Dirac cone-like structure at the \bar{X} point is well visible. In the presented range of energies around the Fermi level we do not observe any surface states coming from the Pb terminated surface. Contrary to this, for the surface (110), both the terminated surfaces allow the realization of the surface states. Here we can distinguish several surface states in

close vicinity of the Fermi level (from both type of terminations).

We also calculate the surface Green's function (spectral function) for semi-infinite system with Pb and Pd termination [panels (c) and (d) on Fig. 4 and Fig. 5, respectively]. In the case of the Pb terminated (110) surface, the surface state form parabolic-like band crossing the Fermi level [marked by green dashed line in Fig. 5(c)]. However, also for deeper energies the surface states are visible as separate sharp lines with high spectral weights (marked by black arrows around -1.5 eV in Fig. 5(c)).

In the case of Pd termination of (001) surface, the earlier mentioned Dirac cone-like structures are also well visible in the spectral function [marked by black arrows in Fig. 4(d)]. For (110) surface, the surface states coming from Pd termination are better visible for several energies at \bar{N} point. Firstly, the parabolic like surface states crossing the Fermi level. Also two separated surface states at 0.5 eV and -1.25 eV are visible [marked by the black arrows in Fig. 5(d)].

As we mentioned above, in the case of the (110) surface, the parabolic-like surface states are well visible in the spectrum. Here it is worth mentioning that this parabolic dispersion relations have different character for Pb termination (electron like) and for Pd termination (hole like).

III. SUMMARY

In summary, we discussed the surface states realized in the Pb_2Pd , for (001) and (110) surfaces terminated by Pb or Pd atoms. As a consequence of dangling bonds of the atoms at the surface, the electronic surface states can be realized. We calculate the surface Green's (spectral) functions for the mentioned surfaces. In the case the (001) surface, the Dirac cone surface states at the \bar{X} point can be observed. However this surface state is located deep down the Fermi surface, and should not play an important role in the physical properties of the Pb_2Pd . Contrary to this, for (110) surface, the surface states can be realized for both termination of the surface. Additionally, the surface states around \bar{N} point, exist in close vicinity of the Fermi surface. Moreover, this states

exhibit parabolic-like relation with different (electron- or hole-like) character. In our opinion, such states should be observed experimentally in a relatively simple way within the ARPES measurements.

ACKNOWLEDGMENTS

Some figures in this work were rendered using VESTA [58] and XCRYSDEN [59] software. S.B. is grateful to IT4Innovations (VŠB-TU Ostrava) for hospitality during a part of the work on this project. This work was supported by the National Science Centre (NCN, Poland) under grants No. 2017/25/B/ST3/02586 (S.B.) and 2021/43/B/ST3/02166 (A.P.). A.P. appreciates funding in the frame of scholarships of the Minister of Science and Higher Education (Poland) for outstanding young scientists (2019 edition, no. 818/STYP/14/2019).

-
- [1] M. Z. Hasan and C. L. Kane, Colloquium: Topological insulators, *Rev. Mod. Phys.* **82**, 3045 (2010).
- [2] X.-L. Qi and S.-C. Zhang, Topological insulators and superconductors, *Rev. Mod. Phys.* **83**, 1057 (2011).
- [3] H. Zhang, C.-X. Liu, X.-L. Qi, X. Dai, Z. Fang, and S.-C. Zhang, Topological insulators in Bi_2Se_3 , Bi_2Te_3 and Sb_2Te_3 with a single Dirac cone on the surface, *Nat. Phys.* **5**, 438 (2009).
- [4] Y. Xia, D. Qian, D. Hsieh, L. Wray, A. Pal, H. Lin, A. Bansil, D. Grauer, Y. S. Hor, R. J. Cava, and M. Z. Hasan, Observation of a large-gap topological-insulator class with a single Dirac cone on the surface, *Nat. Phys.* **5**, 398 (2009).
- [5] Y. L. Chen, J. G. Analytis, J.-H. Chu, Z. K. Liu, S.-K. Mo, X. L. Qi, H. J. Zhang, D. H. Lu, X. Dai, Z. Fang, S. C. Zhang, I. R. Fisher, Z. Hussain, and Z.-X. Shen, Experimental realization of a three-dimensional topological insulator, Bi_2Te_3 , *Science* **325**, 178 (2009).
- [6] Y. L. Chen, J.-H. Chu, J. G. Analytis, Z. K. Liu, K. Igarashi, H.-H. Kuo, X. L. Qi, S. K. Mo, R. G. Moore, D. H. Lu, M. Hashimoto, T. Sasagawa, S. C. Zhang, I. R. Fisher, Z. Hussain, and Z. X. Shen, Massive Dirac fermion on the surface of a magnetically doped topological insulator, *Science* **329**, 659 (2010).
- [7] S.-Y. Xu, M. Neupane, C. Liu, D. Zhang, A. Richardella, L. Andrew Wray, N. Alidoust, M. Leandersson, T. Balasubramanian, J. Sánchez-Barriga, O. Rader, G. Landolt, B. Slomski, J. Hugo Dil, J. Osterwalder, T.-R. Chang, H.-T. Jeng, H. Lin, A. Bansil, N. Samarth, and M. Zahid Hasan, Hedgehog spin texture and Berry's phase tuning in a magnetic topological insulator, *Nature Physics* **8**, 616 (2012).
- [8] A. Ptok, K. J. Kapcia, and A. Ciechan, Electronic properties of Bi_2Se_3 doped by $3d$ transition metal (Mn, Fe, Co, or Ni) ions, *J. Phys.: Condens. Matter* **33**, 065501 (2020).
- [9] M. M. Otrokov, I. I. Klimovskikh, H. Bentmann, D. Estyunin, A. Zeugner, Z. S. Aliev, S. Gaß, A. U. B. Wolter, A. V. Koroleva, A. M. Shikin, M. Blanco-Rey, M. Hoffmann, I. P. Rusinov, A. Y. Vyazovskaya, S. V. Eremeev, Y. M. Koroteev, V. M. Kuznetsov, F. Freyze, J. Sánchez-Barriga, I. R. Amiraslanov, M. B. Babanly, N. T. Mamedov, N. A. Abdullayev, V. N. Zverev, A. Alfonsov, V. Kataev, B. Büchner, E. F. Schwier, S. Kumar, A. Kimura, L. Petaccia, G. Di Santo, R. C. Vidal, S. Schatz, K. Kißner, M. Ünzelmann, C. H. Min, S. Moser, T. R. F. Peixoto, F. Reinert, A. Ernst, P. M. Echenique, A. Isaeva, and E. V. Chulkov, Prediction and observation of an antiferromagnetic topological insulator, *Nature* **576**, 416 (2019).
- [10] Y. Gong, J. Guo, J. Li, K. Zhu, M. Liao, X. Liu, Q. Zhang, L. Gu, L. Tang, X. Feng, D. Zhang, W. Li, C. Song, L. Wang, P. Yu, X. Chen, Y. Wang, H. Yao, W. Duan, Y. Xu, S.-C. Zhang, X. Ma, Q.-K. Xue, and K. He, Experimental realization of an intrinsic magnetic topological insulator, *Chinese Phys. Lett.* **36**, 076801 (2019).
- [11] J.-Q. Yan, Q. Zhang, T. Heitmann, Z. Huang, K. Y. Chen, J.-G. Cheng, W. Wu, D. Vaknin, B. C. Sales, and R. J. McQueeney, Crystal growth and magnetic structure of MnBi_2Te_4 , *Phys. Rev. Materials* **3**, 064202 (2019).
- [12] P. Swatek, Y. Wu, L.-L. Wang, K. Lee, B. Schrnk, J. Yan, and A. Kaminski, Gapless Dirac surface states in the antiferromagnetic topological insulator MnBi_2Te_4 , *Phys. Rev. B* **101**, 161109 (2020).
- [13] S. M. Young, S. Zaheer, J. C. Y. Teo, C. L. Kane, E. J. Mele, and A. M. Rappe, Dirac semimetal in three dimensions, *Phys. Rev. Lett.* **108**, 140405 (2012).
- [14] Z. K. Liu, B. Zhou, Y. Zhang, Z. J. Wang, H. M. Weng, D. Prabhakaran, S.-K. Mo, Z. X. Shen, Z. Fang, X. Dai, Z. Hussain, and Y. L. Chen, Discovery of a three-dimensional topological dirac semimetal, Na_3Bi , *Science* **343**, 864 (2014).
- [15] L. M. Schoop, A. Topp, J. Lippmann, F. Orlandi, L. Müchler, M. G. Vergniory, Y. Sun, A. W. Rost, V. Duppel, M. Krivenkov, S. Sheoran, P. Manuel, A. Varykhalov, B. Yan, R. K. Kremer, C. R. Ast, and B. V. Lotsch, Tunable Weyl and Dirac states in the non-symmorphic compound CeSbTe , *Sci. Adv.* **4**, eaar2317 (2018).

- [16] S.-Y. Xu, I. Belopolski, N. Alidoust, M. Neupane, G. Bian, C. Zhang, R. Sankar, G. Chang, Z. Yuan, C.-C. Lee, S.-M. Huang, H. Zheng, J. Ma, D. S. Sanchez, B. Wang, A. Bansil, F. Chou, P. P. Shibayev, H. Lin, S. Jia, and M. Z. Hasan, Discovery of a Weyl fermion semimetal and topological Fermi arcs, *Science* **349**, 613 (2015).
- [17] H. Weng, C. Fang, Z. Fang, B. A. Bernevig, and X. Dai, Weyl semimetal phase in noncentrosymmetric transition-metal monophosphides, *Phys. Rev. X* **5**, 011029 (2015).
- [18] B. Q. Lv, H. M. Weng, B. B. Fu, X. P. Wang, H. Miao, J. Ma, P. Richard, X. C. Huang, L. X. Zhao, G. F. Chen, Z. Fang, X. Dai, T. Qian, and H. Ding, Experimental discovery of Weyl semimetal TaAs, *Phys. Rev. X* **5**, 031013 (2015).
- [19] Z. Wang, M. G. Vergniory, S. Kushwaha, M. Hirschberger, E. V. Chulkov, A. Ernst, N. P. Ong, R. J. Cava, and B. A. Bernevig, Time-reversal-breaking Weyl fermions in magnetic heusler alloys, *Phys. Rev. Lett.* **117**, 236401 (2016).
- [20] R. Yu, Q. Wu, Z. Fang, and H. Weng, From nodal chain semimetal to Weyl semimetal in HfC, *Phys. Rev. Lett.* **119**, 036401 (2017).
- [21] C. Fang, H. Weng, X. Dai, and Z. Fang, Topological nodal line semimetals, *Chinese Phys. B* **25**, 117106 (2016).
- [22] L. M. Schoop, M. N. Ali, C. Straker, A. Topp, A. Varykhalov, D. Marchenko, V. Duppel, S. S. P. Parkin, B. V. Lotsch, and C. R. Ast, Dirac cone protected by non-symmorphic symmetry and three-dimensional dirac line node in zrsis, *Nature Communications* **7**, 11696 (2016).
- [23] D. Takane, Z. Wang, S. Souma, K. Nakayama, C. X. Trang, T. Sato, T. Takahashi, and Y. Ando, Dirac-node arc in the topological line-node semimetal HfSiS, *Phys. Rev. B* **94**, 121108 (2016).
- [24] C. Chen, X. Xu, J. Jiang, S.-C. Wu, Y. P. Qi, L. X. Yang, M. X. Wang, Y. Sun, N. B. M. Schröter, H. F. Yang, L. M. Schoop, Y. Y. Lv, J. Zhou, Y. B. Chen, S. H. Yao, M. H. Lu, Y. F. Chen, C. Felser, B. H. Yan, Z. K. Liu, and Y. L. Chen, Dirac line nodes and effect of spin-orbit coupling in the nonsymmorphic critical semimetals $MSiS$ ($M = \text{Hf, Zr}$), *Phys. Rev. B* **95**, 125126 (2017).
- [25] M. M. Hosen, K. Dimitri, I. Belopolski, P. Maldonado, R. Sankar, N. Dhakal, G. Dhakal, T. Cole, P. M. Oppeneer, D. Kaczorowski, F. Chou, M. Z. Hasan, T. Durakiewicz, and M. Neupane, Tunability of the topological nodal-line semimetal phase in $ZrSiX$ -type materials ($X = \text{S, Se, Te}$), *Phys. Rev. B* **95**, 161101 (2017).
- [26] R. Wang, J. Z. Zhao, Y. J. Jin, Y. P. Du, Y. X. Zhao, H. Xu, and S. Y. Tong, Nodal line fermions in magnetic oxides, *Phys. Rev. B* **97**, 241111 (2018).
- [27] B.-B. Fu, C.-J. Yi, T.-T. Zhang, M. Caputo, J.-Z. Ma, X. Gao, B. Q. Lv, L.-Y. Kong, Y.-B. Huang, P. Richard, M. Shi, V. N. Strocov, C. Fang, H.-M. Weng, Y.-G. Shi, T. Qian, and H. Ding, Dirac nodal surfaces and nodal lines in $ZrSiS$, *Sci. Adv.* **5**, eaau6459 (2019).
- [28] M. Gendron and R. Jones, Superconductivity in the CuAl_2 (C16) crystal class, *J. Phys. Chem. Solids* **23**, 405 (1962).
- [29] M. M. Sharma, N. K. Karn, P. Rani, R. N. Bhowmik, and V. P. S. Awana, Bulk superconductivity and non-trivial band topology analysis of Pb_2Pd , *Supercond. Sci. Technol.* **35**, 084010 (2022).
- [30] M. Wang and K. Tang, Bi substitution effect on superconductivity of novel Pb_2Pd alloy, *Phys. C* **565**, 1353518 (2019).
- [31] H. Leng, J.-C. Orain, A. Amato, Y. K. Huang, and A. de Visser, Type-I superconductivity in the Dirac semimetal PdTe_2 probed by μSR , *Phys. Rev. B* **100**, 224501 (2019).
- [32] Arushi, K. Motla, A. Kataria, S. Sharma, J. Beare, M. Pula, M. Nugent, G. M. Luke, and R. P. Singh, Type-I superconductivity in single-crystal Pb_2Pd , *Phys. Rev. B* **103**, 184506 (2021).
- [33] F. Martín-Vega, E. Herrera, B. Wu, V. Barrena, F. Mompeán, M. García-Hernández, P. C. Canfield, A. M. Black-Schaffer, J. J. Baldoví, I. Guillamón, and H. Suderow, Superconducting density of states and band structure at the surface of the candidate topological superconductor Au_2Pb , *Phys. Rev. Research* **4**, 023241 (2022).
- [34] N. Kumar, M. Yao, J. Nayak, M. G. Vergniory, J. Bannies, Z. Wang, N. B. M. Schröter, V. N. Strocov, L. Müchler, W. Shi, E. D. L. Rienks, J. L. Mañes, C. Shekhar, S. S. P. Parkin, J. Fink, G. H. Fecher, Y. Sun, B. A. Bernevig, and C. Felser, Signatures of sixfold degenerate exotic fermions in a superconducting metal PdSb_2 , *Adv. Mater.* **32**, 1906046 (2020).
- [35] Y. Liu, J.-Z. Zhao, L. Yu, C.-T. Lin, A.-J. Liang, C. Hu, Y. Ding, Y. Xu, S.-L. He, L. Zhao, G.-D. Liu, X.-L. Dong, J. Zhang, C.-T. Chen, Z.-Y. Xu, H.-M. Weng, X. Dai, Z. Fang, and X.-J. Zhou, Identification of topological surface state in PdTe_2 superconductor by angle-resolved photoemission spectroscopy, *Chinese Phys. Lett.* **32**, 067303 (2015).
- [36] F. Fei, X. Bo, R. Wang, B. Wu, J. Jiang, D. Fu, M. Gao, H. Zheng, Y. Chen, X. Wang, H. Bu, F. Song, X. Wan, B. Wang, and G. Wang, Nontrivial Berry phase and type-II Dirac transport in the layered material PdTe_2 , *Phys. Rev. B* **96**, 041201 (2017).
- [37] H.-J. Noh, J. Jeong, E.-J. Cho, K. Kim, B. I. Min, and B.-G. Park, Experimental realization of type-II Dirac fermions in a PdTe_2 superconductor, *Phys. Rev. Lett.* **119**, 016401 (2017).
- [38] M. S. Bahramy, O. J. Clark, B.-J. Yang, J. Feng, L. Bawden, J. M. Riley, I. Marković, F. Mazzola, V. Sunko, D. Biswas, S. P. Cooil, M. Jorge, J. W. Wells, M. Leandersson, T. Balasubramanian, J. Fujii, I. Vobornik, J. E. Rault, T. K. Kim, M. Hoesch, K. Okawa, M. Asakawa, T. Sasagawa, T. Eknapakul, W. Meevasana, and P. D. C. King, Ubiquitous formation of bulk Dirac cones and topological surface states from a single orbital manifold in transition-metal dichalcogenides, *Nat. Mater.* **17**, 28 (2018).
- [39] K. Iwaya, Y. Kohsaka, K. Okawa, T. Machida, M. S. Bahramy, T. Hanaguri, and T. Sasagawa, Full-gap superconductivity in spin-polarised surface states of topological semimetal $\beta\text{-PdBi}_2$, *Nat. Commun.* **8**, 976 (2017).
- [40] P.-F. Liu, J. Li, X.-H. Tu, H. Yin, B. Sa, J. Zhang, D. J. Singh, and B.-T. Wang, Prediction of superconductivity and topological aspects in single-layer $\beta\text{-Bi}_2\text{Pd}$, *Phys. Rev. B* **102**, 155406 (2020).
- [41] P. E. Blöchl, Projector augmented-wave method, *Phys. Rev. B* **50**, 17953 (1994).
- [42] G. Kresse and J. Hafner, Ab initio molecular-dynamics simulation of the liquid-metal–amorphous-semiconductor transition in germanium, *Phys. Rev. B* **49**, 14251 (1994).

- [43] G. Kresse and J. Furthmüller, Efficient iterative schemes for ab initio total-energy calculations using a plane-wave basis set, *Phys. Rev. B* **54**, 11169 (1996).
- [44] G. Kresse and D. Joubert, From ultrasoft pseudopotentials to the projector augmented-wave method, *Phys. Rev. B* **59**, 1758 (1999).
- [45] J. P. Perdew, K. Burke, and M. Ernzerhof, Generalized gradient approximation made simple, *Phys. Rev. Lett.* **77**, 3865 (1996).
- [46] H. J. Monkhorst and J. D. Pack, Special points for Brillouin-zone integrations, *Phys. Rev. B* **13**, 5188 (1976).
- [47] H. T. Stokes and D. M. Hatch, FINDSYM: program for identifying the space-group symmetry of a crystal, *J. Appl. Crystallogr.* **38**, 237 (2005).
- [48] Y. Hinuma, G. Pizzi, Y. Kumagai, F. Oba, and I. Tanaka, Band structure diagram paths based on crystallography, *Comput. Mater. Sci.* **128**, 140 (2017).
- [49] A. Togo and I. Tanaka, Spglib: a software library for crystal symmetry search (2018), [arXiv:1808.01590](https://arxiv.org/abs/1808.01590).
- [50] N. Marzari, A. A. Mostofi, J. R. Yates, I. Souza, and D. Vanderbilt, Maximally localized Wannier functions: Theory and applications, *Rev. Mod. Phys.* **84**, 1419 (2012).
- [51] N. Marzari and D. Vanderbilt, Maximally localized generalized Wannier functions for composite energy bands, *Phys. Rev. B* **56**, 12847 (1997).
- [52] I. Souza, N. Marzari, and D. Vanderbilt, Maximally localized Wannier functions for entangled energy bands, *Phys. Rev. B* **65**, 035109 (2001).
- [53] A. A. Mostofi, J. R. Yates, Y.-S. Lee, I. Souza, D. Vanderbilt, and N. Marzari, WANNIER90: A tool for obtaining maximally-localised wannier functions, *Comput. Phys. Commun.* **178**, 685 (2008).
- [54] A. A. Mostofi, J. R. Yates, G. Pizzi, Y.-S. Lee, I. Souza, D. Vanderbilt, and N. Marzari, An updated version of WANNIER90: A tool for obtaining maximally-localised wannier functions, *Comput. Phys. Commun.* **185**, 2309 (2014).
- [55] G. Pizzi, V. Vitale, R. Arita, S. Blügel, F. Freimuth, G. Géranton, M. Gibertini, D. Gresch, C. Johnson, T. Koretsune, J. Ibañez-Azpiroz, H. Lee, J.-M. Lihm, D. Marchand, A. Marrazzo, Y. Mokrousov, J. I. Mustafa, Y. Nohara, Y. Nomura, L. Paulatto, S. Poncé, T. Ponweiser, J. Qiao, F. Thöle, S. S. Tsirkin, M. Wierzbowska, N. Marzari, D. Vanderbilt, I. Souza, A. A. Mostofi, and J. R. Yates, WANNIER90 as a community code: new features and applications, *J. Phys.: Condens. Matter* **32**, 165902 (2020).
- [56] M. P. L. Sancho, J. M. L. Sancho, J. M. L. Sancho, and J. Rubio, Highly convergent schemes for the calculation of bulk and surface Green functions, *J. Phys. F: Met. Phys.* **15**, 851 (1985).
- [57] Q. S. Wu, S. N. Zhang, H.-F. Song, M. Troyer, and A. A. Soluyanov, WANNIERTOOLS: An open-source software package for novel topological materials, *Comput. Phys. Commun.* **224**, 405 (2018).
- [58] K. Momma and F. Izumi, VESTA3 for three-dimensional visualization of crystal, volumetric and morphology data, *J. Appl. Crystallogr.* **44**, 1272 (2011).
- [59] A. Kokalj, XCRYSDEN—a new program for displaying crystalline structures and electron densities, *J. Mol. Graph. and Model.* **17**, 176 (1999).